PCCP

PAPER

View Article Online
View Journal | View Issue

Cite this: *Phys. Chem. Chem. Phys.*, 2025, **27**, 16123

Precision measurements of absolute line strengths of the HO_2 radical in the ν_1 and ν_2 vibrational bands†

I-Yun Chen,‡[ab] Che-Wei Chang,‡[acd] Qian-Rui Huang,[a] Jer-Lai Kuo[a] and Pei-Ling Luo*[a]

The hydroperoxy radical (HO_2), a key species in atmospheric chemistry, necessitates accurate quantitative measurements and precise spectroscopic characterization, both of which are essential for laboratory investigations and field observations. Herein, we present precision measurements of the absolute line strengths of the HO_2 radical in the ν_1 and ν_2 vibrational bands by utilizing synchronized two-color time-resolved dual-comb spectroscopy in the mid-infrared region. By simultaneously measuring the byproduct HCl near 3.3 μm and the HO_2 radical near 7.1 μm following flash photolysis of $Cl_2/CH_3OH/O_2$ gas mixtures, we were able to determine the absolute line intensities for several HO_2 ν_2 transitions, using the well-known line strength of HCl as a reference. Furthermore, the line intensities for the HO_2 ν_1 transitions were obtained relative to the accurately characterized line strengths of the HO_2 ν_3 or ν_2 transitions, by simultaneous probing of the HO_2 radical in the ν_1 band (2.9 μm) and either the ν_3 band (8.9 μm) or the ν_2 band (7.1 μm). Through high-resolution spectral analysis based on the vibration–rotation parameters of HO_2, the absolute intensities of the ν_1 and ν_2 vibrational bands of HO_2 were determined to be 18.5 ± 1.5 and 26.6 ± 1.3 km mol^{-1}, respectively. Additionally, the HO_2 fundamental band strengths were calculated using different levels of theory, and compared with the experimental results. This work presents precise experimental data together with theoretical comparisons of the absolute line strengths of HO_2, contributing to the revision of the spectral database for the HO_2 radical and supporting the validation of computational methods for predicting infrared intensities of radical vibrational bands.

Received 13th May 2025,
Accepted 2nd July 2025

DOI: 10.1039/d5cp01784j

rsc.li/pccp

1. Introduction

The hydroperoxy radical (HO_2) plays a pivotal role in HO_x and NO_x cycling reactions, thereby influencing the atmospheric oxidizing capacity.[1–5] As a key molecule in atmospheric chemistry, HO_2 has long been recognized for its significance and is routinely monitored in field observations[2–5] as well as in numerous laboratory kinetic investigations.[6–8] Therefore, precise spectroscopic studies of the HO_2 radical are essential for accurately determining its concentration in both laboratory and field measurements. Various studies of HO_2 spectroscopic characterization have been conducted in ultraviolet,[9] near infrared,[10] mid-infrared,[11–14] and microwave regions[15] to investigate its $\tilde{B}$–$\tilde{X}$ and $\tilde{A}$–$\tilde{X}$ electronic transitions, vibrational–rotational spectra in the fundamental bands, and rotational transitions in the ground vibronic state, respectively. As an asymmetric-top molecule, HO_2 has three fundamental vibrational modes: O–H stretching (ν_1), bending (ν_2), and O–O stretching (ν_3) bands at 3436, 1392, and 1098 cm^{-1}, respectively. According to early spectroscopic studies,[11–15] the vibration–rotation parameters of ground and excited vibronic states were determined with high accuracy, and most of the strong fundamental transitions were appropriately assigned; however, precise measurements of the line strengths of HO_2 fundamental transitions are still lacking. In an early experimental study, Zahniser and Stanton carried out the band strength measurement of the HO_2 ν_3 band using the $F + H_2O_2 \rightarrow HO_2 + HF$

[a] *Institute of Atomic and Molecular Sciences Academia Sinica, Taipei 106319, Taiwan. E-mail: plluo@gate.sinica.edu.tw*
[b] *Department of Chemistry, National Taiwan University, Taipei 10617, Taiwan*
[c] *Molecular Science and Technology Program, Taiwan International Graduate Program, Academia Sinica, Taipei, 11529, Taiwan*
[d] *International Graduate Program of Molecular Science and Technology, National Taiwan University, Taipei, 10617, Taiwan*

† Electronic supplementary information (ESI) available: Data distributions of measured intensities for several HO_2 ν_2 and ν_1 transitions, simulated spectra of the ν_2 and ν_1 bands, time-dependent high-resolution spectra of the HO_2 ν_1 band, comparisons of the temporal profiles of the HO_2 ν_1, ν_2, and ν_3 transitions, vibration–rotation parameters of HO_2, summary of all experimental conditions, summary of HO_2 ν_2 and ν_1 line strengths, and summary of the HO_2 vibrational frequencies and band strengths obtained from different computational methods. See DOI: https://doi.org/10.1039/d5cp01784j

‡ I-Y. Chen and C.-W. Chang contributed equally.

reaction in a discharge-flow system.[16] By calibrating the HO_2 concentration based on the determined F atom concentration, they reported a HO_2 ν_3 band strength of 7.8 ± 2.0 km mol^{-1}. Subsequently, Zahniser *et al.* also performed relative intensity measurements of HO_2 lines in the ν_2 and ν_3 bands, as well as in the ν_1 and ν_2 bands. By combining these measurements with the calculated ratios of single-line to entire-band strength, they derived the ν_1 and ν_2 band strengths to be 4.5 ± 1.3 km mol^{-1} and 13.0 ± 3.6 km mol^{-1}, respectively.[17] However, the early experimental results were significantly lower than theoretical predictions, although the theoretical values themselves varied widely depending on the computational methods used.[18,19] More recently, Sakamoto and Tonokura determined the HO_2 ν_3 band strength by quantifying HO_2 through its self-reaction kinetics or the depletion of CH_3OH in a flash photolysis system of $Cl_2/CH_3OH/O_2$ mixtures and then combined the vibrational–rotational spectral analysis to derive the ν_3 band strength of 21.4 ± 4.2 km mol^{-1},[20] approximately three times higher than the value reported by Zahniser and Stanton. In our previous work on the absolute line strengths of HO_2 in the ν_3 fundamental band, the line strength of the ν_3 $13_{1,13} \leftarrow 12_{1,12}$ $F_{1,2}$ transitions was accurately determined relative to the HCl R(9) transition by simultaneously measuring the time-resolved difference absorbance spectra of HO_2 and HCl near 8.9 and 3.3 μm, respectively.[21] Based on the spectral analysis of hundreds of rovibrational transitions in the HO_2 ν_3 band, the ν_3 band strength was derived to be 22.3 ± 1.1 km mol^{-1}, which agrees with the recent value reported by Sakamoto and Tonokura, further confirming the discrepancy with earlier experimental results. As for the line strengths in the ν_1 and ν_2 fundamental bands, only one experimental study was conducted so far by Zahniser *et al.*[17] Although the band strength ratio of ν_1, ν_2 and ν_3 was reported to be approximately 0.6 : 1.7 : 1.0, it was estimated based on the theoretically calculated ratios of single-line to entire-band strength, making its accuracy difficult to assess.

In this work, we extended our previous work on the absolute line strengths of HO_2 by employing synchronized two-color time-resolved dual-comb spectroscopy coupled with the flash photolysis system. By operating two sets of dual-comb lasers near 7.1 and 3.3 μm, HO_2 transitions in the ν_2 band and the HCl R(9) line could be simultaneously measured upon irradiation of $Cl_2/CH_3OH/O_2$ flowing mixtures at 351 nm. The absolute line strengths of several ν_2 transitions near 1407 and 1411 cm^{-1} were directly determined relative to the precisely known line strength of HCl. Additionally, by simultaneously probing the HO_2 radical in the ν_1 band near 2.9 μm, and either the ν_3 band near 8.9 μm or the ν_2 band near 7.1 μm, the absolute line intensities of several HO_2 ν_1 transitions near 3456 and 3415 cm^{-1} were determined relative to the accurately characterized line strengths of the HO_2 ν_3 $13_{1,13} \leftarrow 12_{1,12}$ $F_{1,2}$ transitions at 1122.983 cm^{-1} or the ν_2 $7_{1,6} \leftarrow 6_{1,5}$ $F_{1,2}$ transitions at 1407.620 cm^{-1}. The high-resolution spectra of HO_2 in the range of 3433.90–3468.90 cm^{-1} were also recorded with an averaged resolution of 0.002 cm^{-1}, and both the a- and b-type transitions in the ν_1 band were experimentally identified for the first time. Through spectral analysis using the determined vibration–rotation parameters, the band strengths of the fundamental vibrational bands of HO_2 were derived and also compared with the results from quantum chemical calculations.

2. Experimental methods

Herein, we performed absolute line strength measurements of the HO_2 radical by detecting both the stable products HCl and HO_2 or by simultaneously probing HO_2 in different vibrational bands. HO_2 was produced from the reactions of Cl + CH_3OH → CH_2OH + HCl and CH_2OH + O_2 → HO_2 + HCHO, in which the Cl atoms can be efficiently generated by photolysis of Cl_2 at 351 nm. According to our previous estimations using a kinetic model that accounts for the HO_2 self-reaction and all other side reactions, the HO_2 concentration was found to closely match that of the HCl in the early stage of the reaction (25–100 μs), under conditions of low initial Cl concentration and excess O_2.[21] A slight concentration difference of less than 1% was estimated in the kinetic simulations when $[Cl]_0 < 2 \times 10^{13}$ molecule cm^{-3} and $[O_2]_0 = 1.3 \times 10^{18}$ molecule cm^{-3}. Therefore, the absolute line strengths of the HO_2 transitions could be determined based on the accurately known line strength of HCl as a reference and were derived using the following formula:

$$S_{HO_2} = S_{HCl} \times \frac{[\text{Int. } \Delta\text{Abs.}]_{HO_2,es}}{[\text{Int. } \Delta\text{Abs.}]_{HCl,es}} \quad (1)$$

where S_{HO_2} and S_{HCl} represent the line strengths of the measured HO_2 and HCl transitions, respectively. $[\text{Int. } \Delta\text{Abs.}]_{HO_2,es}$ and $[\text{Int. } \Delta\text{Abs.}]_{HCl,es}$ represent the integrated difference absorbance areas of the HO_2 and HCl absorption lines, respectively, obtained in the early stage of the reaction. Using this approach, we previously achieved absolute line strength measurements of the HO_2 ν_3 $13_{1,13} \leftarrow 12_{1,12}$ $F_{1,2}$ transitions and reported an uncertainty of 4%.[21] In this work, building on a similar approach, the absolute line intensities of the HO_2 ν_2 transitions were determined relative to the HCl line strength. On the other hand, the line intensities of the HO_2 transitions in the ν_1 band could be obtained by referencing the accurately characterized line strengths of the HO_2 ν_3 or ν_2 transitions.

Fig. 1 shows a schematic of the experimental setup. A short-wave mid-infrared dual-comb laser, constructed through difference frequency generation (DFG) between an electro-optic dual-comb laser (EODCS) at 1050 nm and a tunable diode laser in the 765–800 nm region, was operated either near 3.3 μm to measure the HCl R(9) line at 3059.316 cm^{-1} or near 2.9 μm to measure the HO_2 ν_1 transitions. Another long-wave mid-infrared dual-comb source, generated by DFG between the tunable EODCS in the 1530–1600 nm region and fiber lasers at 1915 or 1999 nm, was operated either near 7.1 μm to probe the HO_2 lines in the ν_2 band or near 8.9 μm to measure the HO_2 ν_3 $13_{1,13} \leftarrow 12_{1,12}$ $F_{1,2}$ transitions at 1122.983 cm^{-1}. Both the short-wave and long-wave mid-infrared dual-comb lasers were operated in synchronization and coupled into a multipass reactor cell. A 351 nm excimer laser, used as the photolysis laser, was directed through the center of the reactor cell to

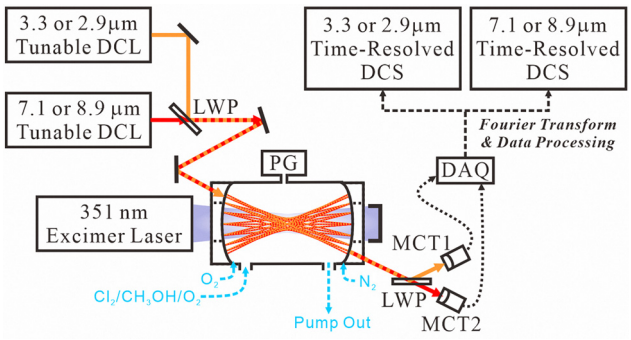

Fig. 1 Schematic diagram of the experimental setup. DCL: dual-comb laser, LWP: longwave pass filter, PG: pressure gauge, MCT: HgCdTe detector, DAQ: data acquisition board, and DCS: dual-comb spectra.

initiate the reactions. Following photolysis, time-resolved dual-comb spectra were simultaneously recorded in both the short-wave and long-wave mid-infrared ranges. Fig. 2 shows the representative time-resolved dual-comb spectra in the four different mid-infrared spectral regions of 3059.05–3059.48 cm^{-1} (near 3.3 μm), 1407.56–1408.02 cm^{-1} (near 7.1 μm), 3456.17–3456.60 cm^{-1} (near 2.9 μm), and 1122.78–1123.10 cm^{-1} (near 8.9 μm). The detailed approach of time-resolved dual-comb spectroscopy has been described in our previous works.[22–24] The temporal resolution of time-resolved dual-comb spectroscopy can be adjusted from the μs to the ms level by setting the length of a dual-comb interferogram used to generate each time-dependent Fourier transform (FT) spectrum. By interleaving multiple dual-comb spectra recorded with different central wavelengths and spectral sampling spacings, the rovibrational transitions of the probed species can be analyzed with sufficient resolution, typically better than 0.002 cm^{-1}.

In the experiment for the line intensity measurements of HO_2 ν_2 transitions, we performed two-color time-resolved dual-comb spectroscopy at 3.3 and 7.1 μm to probe HCl and HO_2, respectively, as shown in Fig. 2(a) and (b). For the determination of the HO_2 ν_1 line strengths, two dual-comb lasers were set near 2.9 and 8.9 μm to record the spectra of the HO_2 ν_1 and ν_3 transitions, respectively, as shown in Fig. 2(c) and (d). The line strengths of the HO_2 ν_1 lines could also be determined by simultaneously measuring the ν_1 and ν_2 lines near 2.9 and 7.1 μm for cross confirmation.

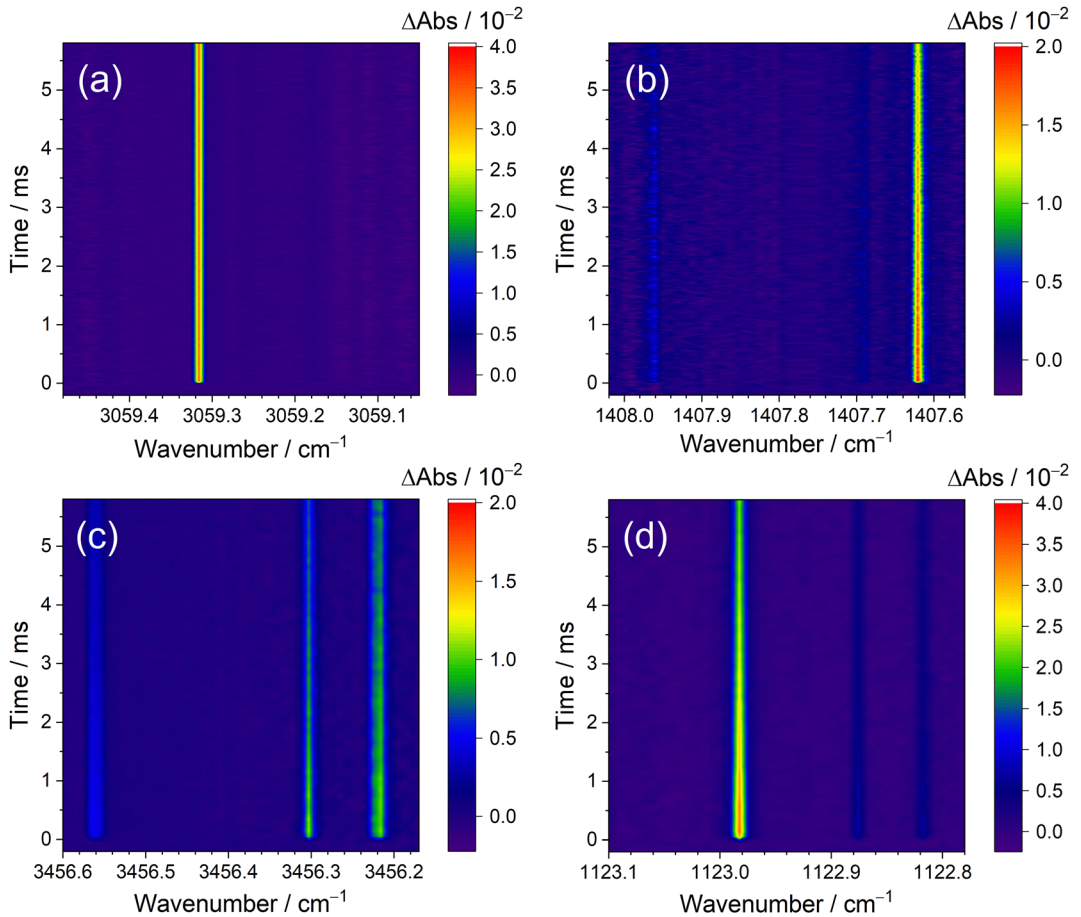

Fig. 2 Representative time-resolved dual-comb spectra in the regions: (a) 3059.05–3059.48, (b) 1407.56–1408.02, (c) 3456.17–3456.60, and (d) 1122.78–1123.10 cm^{-1}. The spectra (a) and (b) were measured simultaneously after the 351 nm irradiation of a flowing mixture of $Cl_2/CH_3OH/O_2$ (0.03/0.12/38.2, P_T = 38.3 torr, and 296 K) over 5000 excimer laser shots. The spectral sampling spacing is 291 MHz (9.7×10^{-3} cm^{-1}), and the temporal resolution is 25 μs. The spectra (c) and (d) were obtained at the same time after the 351 nm irradiation of a flowing mixture of $Cl_2/CH_3OH/O_2$ (0.04/0.04/37.9, P_T = 37.9 torr, and 296 K) over 3000 excimer laser shots. The spectral sampling spacing is 291 MHz (9.7×10^{-3} cm^{-1}), and the temporal resolution is 100 μs.

3. Results and discussion

3.1 Determination of the line intensity of HO_2 fundamental transitions near 7.1 μm and the ν_2 band strength

To determine the absolute line strength of HO_2 ν_2 fundamental transitions near 7.1 μm by referring it to the HCl fundamental transition near 3.3 μm, we conducted experiments at low radical concentrations ($[Cl]_0$ = 1.12–1.26 × 10^{13} molecule cm^{-3}) to suppress the effects of side reactions and to ensure that the concentration differences between HCl and HO_2 remained below 1% at 25–100 μs after laser photolysis. Fig. 3 displays the high-resolution difference absorbance spectra in the ranges of 3059.24−3059.38 cm^{-1} and 1407.56–1408.02 cm^{-1}, respectively, at 25–100 μs after 351 nm laser photolysis of the flowing mixture of $Cl_2/CH_3OH/O_2$ (0.03/0.12/38.3, P_T = 38.4 torr, and 296 K). These high-resolution spectra were obtained by interleaving multiple time-resolved dual-comb spectra and were curve-fitted using a multi-peak Voigt function to derive the integrated absorbance areas of the absorption lines. In the spectral range of 3059.24−3059.38 cm^{-1}, the HCl R(9) line with a line strength of 2.07 × 10^{-20} cm $molecule^{-1}$ was observed, as shown in Fig. 3(a), and used to determine the line strengths of HO_2 transitions in the ν_2 band.

To avoid the effects of strong ambient water absorption and to obtain the spectra with high signal-to-noise ratios (SNR), two spectral ranges near 1407.8 and 1411.1 cm^{-1} were selected for measuring the HO_2 ν_2 transitions in this experiment. In the spectral range of 1407.56–1408.02 cm^{-1}, three HO_2 absorption peaks, corresponding to the ν_2 $5_{3,3} \leftarrow 4_{3,2}$ F_1 and $5_{3,2} \leftarrow 4_{3,1}$ F_1 transitions at 1407.963 cm^{-1}, the $5_{3,3} \leftarrow 4_{3,2}$ F_2 and $5_{3,2} \leftarrow 4_{3,1}$ F_2 transitions at 1407.693 cm^{-1}, and the ν_2 $7_{1,6} \leftarrow 6_{1,5}$ $F_{1,2}$ transitions at 1407.620 cm^{-1}, were obtained, as shown in Fig. 3(b). Additionally, measurements of three other HO_2 absorption peaks were performed, corresponding to the ν_2 $9_{0,9} \leftarrow 8_{0,8}$ F_1 transition at 1410.928 cm^{-1}, the $9_{0,9} \leftarrow 8_{0,8}$ F_2 transition at 1410.941 cm^{-1}, and the ν_2 $9_{1,9} \leftarrow 8_{1,8}$ $F_{1,2}$ transitions at 1411.182 cm^{-1}. By analyzing the high-resolution spectra of HCl and HO_2, and using the accurately known line strength of HCl along with eqn (1), the absolute line strengths of six HO_2 absorption peaks in the ν_2 band were determined. Fig. S1 (ESI†) shows the statistical distributions of multiple measurements of the line strength for the six HO_2 absorption peaks in the ν_2 band. A summary of each experimental condition is listed in Table S1 (ESI†). Taking into account the errors from statistical and spectral analyses (2.5–6.3%), the known uncertainty of S_{HCl} (0.15%),[25] the temperature uncertainty (0.2%), and the concentration difference between HCl and HO_2 (<1%), the absolute line strengths of the HO_2 ν_2 transitions were obtained through direct measurements, with overall uncertainties ranging from 3.5% to 7.3%, depending on the SNR of the measured HO_2 absorption peaks.

Based on early spectroscopic studies, the rotational parameters of HO_2 in the ground state were accurately determined by Charo and Lucia using millimeter and submillimeter spectroscopy.[15] The absorption spectra of the ν_2 fundamental band of HO_2 were later recorded in the spectral range of 1340–1450 cm^{-1} by Burkholder *et al.* using a high resolution Fourier transform spectrometer at a resolution of 0.01 cm^{-1}.[12] Over 400 absorption lines were assigned to the HO_2 ν_2 transitions, enabling the accurate determination of the vibration–rotation parameters of the ν_2 state, as listed in Table S2 (ESI†). Since only the a-type transitions in the ν_2 band were observed in both early experiments[11,12] and our measurements and the intensity contribution of a-type transitions was predicted to exceed 97% based on our theoretical calculations, we hence evaluated the ν_2 band strength based solely on the a-type transitions. Using the previously determined vibration–rotation parameters and the PGOPHER program,[26] we simulated the entire ν_2 band spectrum in the

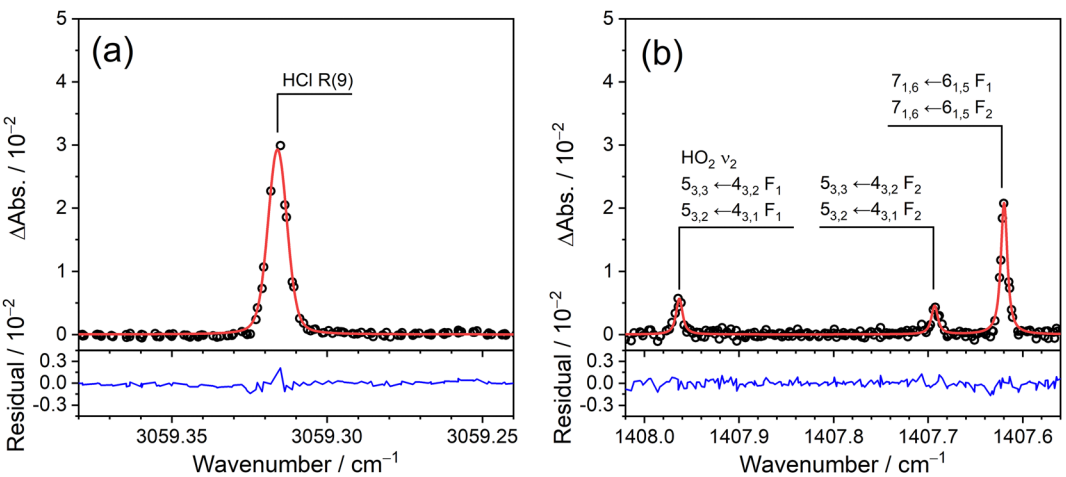

Fig. 3 High-resolution difference absorbance spectra in the regions of (a) 3059.24−3059.38 cm^{-1} and (b) 1407.56–1408.02 cm^{-1}. The spectra (black open circles) were obtained by interleaving over 4 dual-comb spectra recorded with spectral sampling spacings of 279 MHz (9.3 × 10^{-3} cm^{-1}) and 291 MHz (9.7 × 10^{-3} cm^{-1}) at 25–100 μs after photolysis of the flowing mixture of $Cl_2/CH_3OH/O_2$ (0.03/0.12/38.3, P_T = 38.4 torr, and 296 K) at 351 nm with a photolysis energy of 22.6 mJ cm^{-2}. Here, the initial concentration of the Cl radical, $[Cl]_0$, is 1.20 × 10^{13} molecule cm^{-3}. The observed spectra were fitted using a multi-peak Voigt function (red curves) to obtain the integrated absorbance areas of the absorption peaks of HCl and HO_2. The bottom panels show the fitting residuals.

1250–1550 cm^{-1} range (Fig. S2, ESI†) and subsequently obtained the absolute line strengths of all individual ro-vibrational transitions within this spectral range, relative to the well-determined line strength of the ν_2 $7_{1,6} \leftarrow 6_{1,5}$ $F_{1,2}$ transitions at 1407.620 cm^{-1}. The line strength of each individual ν_2 transition obtained from PGOPHER simulations are in good agreement with the values from our direct measurements, as shown in Table 1. Notably, our measured line strengths of the HO_2 ν_2 transition are approximately twice as large as those reported in the earlier study by Zahniser *et al.*[17] and the values listed in the HITRAN database.[27] Table S3 (ESI†) lists the HO_2 ν_2 transitions with the line strengths of $>3 \times 10^{-22}$ cm molecule^{-1} in the spectral region of 1340–1450 cm^{-1} and Fig. 4 presents a comparison of the HO_2 ν_2 transition line strengths determined in this work with the corresponding values from the HITRAN database. The line strengths obtained in this work are higher than those in the HITRAN database by factors ranging from 2.11 to 1.95 in the 1340–1450 cm^{-1} region, exhibiting a linearly decreasing trend in the difference factor with an increasing transition frequency.

The ν_2 band strength was determined to be 26.6 ± 1.3 km mol^{-1} by summing the relative line strengths of all ro-vibrational transitions obtained from PGOPHER simulations over the 1250–1550 cm^{-1} range and scaling the total based on the experimentally measured absolute line strength of the $7_{1,6} \leftarrow 6_{1,5}$ $F_{1,2}$ transitions at 1407.620 cm^{-1}. The overall error of the ν_2 band strength (4.9%) was estimated by considering the standard deviation (3.5%) of the difference between the experimental values obtained from PGOPHER simulations and direct measurements, as well as the uncertainty in the determined line strength of the ν_2 $7_{1,6} \leftarrow 6_{1,5}$ $F_{1,2}$ transitions (3.5%).

3.2 Determination on the line intensity of HO_2 fundamental transitions near 2.9 μm and the ν_1 band strength

To determine the line strengths of the HO_2 ν_1 fundamental transitions, we conducted experiments by simultaneously probing HO_2 in the ν_1 band near 2.9 μm and in either the ν_3 band near 8.9 μm or the ν_2 band near 7.1 μm. Since the normalized temporal profiles of all HO_2 fundamental transitions were observed to be identical under the same experimental conditions (as shown in Fig. S3, ESI†), the line strength of the HO_2 ν_1 transitions could be determined by directly referencing our previously measured line strengths of the ν_3 or ν_2 transitions. Additionally, slightly higher initial concentrations of Cl radicals ($[Cl]_0$ = 1.38–3.03 × 10^{13} molecule cm^{-3}) were used in the experiments to obtain the spectra with a higher SNR. Fig. 5 shows the high-resolution difference absorbance spectra in the ranges of 3415.22–3415.76 cm^{-1} and 1122.75–1123.07 cm^{-1}, respectively, at 100–200 μs after 351 nm laser photolysis of the flowing mixture of $Cl_2/CH_3OH/O_2$ (0.04/0.04/37.8 torr, P_T = 37.9 torr, and 296 K). These spectra were obtained by interleaving four time-resolved dual-comb spectra and were curve-fitted using a multi-peak Voigt function to derive the integrated absorbance area of each HO_2 absorption peak. In the spectral range of 3415.22–3415.76 cm^{-1}, four HO_2 absorption peaks, corresponding to the ν_1 $0_{0,0} \leftarrow 1_{1,1}$ F_1

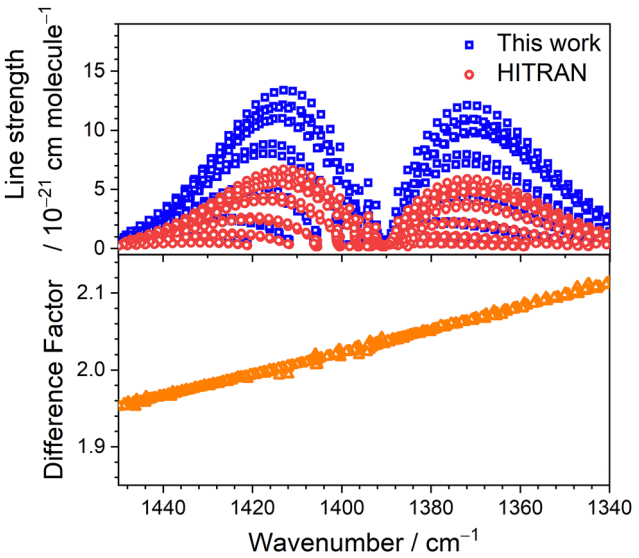

Fig. 4 Comparison of the line strengths of the HO_2 ν_2 transitions determined in this work and those listed in the HITRAN database.[27] The transitions with the obtained line strengths of $>3 \times 10^{-22}$ cm molecule^{-1} in the spectral region of 1340–1450 cm^{-1} are only shown here.

Table 1 Comparison of line intensities for the HO_2 ν_2 transitions

		Line intensity/10^{-21} cm molecule^{-1}			
Line position/cm^{-1}	Transition	HITRAN[27]	Zahniser *et al.*[17]	This work *via* PGOPHER simulations[a]	This work from direct measurements[b]
1407.620	$7_{1,6} \leftarrow 6_{1,5}$ F_1	10.5[c]		20.4[c]	20.4 ± 0.71[c]
	$7_{1,6} \leftarrow 6_{1,5}$ F_2				
1407.693	$5_{3,3} \leftarrow 4_{3,2}$ F_2	2.34[c]		4.71[c]	4.47 ± 0.31[c]
	$5_{3,2} \leftarrow 4_{3,1}$ F_2				
1407.963	$5_{3,3} \leftarrow 4_{3,2}$ F_1	2.71[c]		5.45[c]	5.33 ± 0.31[c]
	$5_{3,2} \leftarrow 4_{3,1}$ F_1				
1410.928	$9_{0,9} \leftarrow 8_{0,8}$ F_1	6.64		13.3	13.7 ± 0.99
1410.941	$9_{0,9} \leftarrow 8_{0,8}$ F_2	5.93		11.9	12.1 ± 0.51
1411.182	$9_{1,9} \leftarrow 8_{1,8}$ F_1	11.4[c]	11.6[c]	22.8[c]	23.8 ± 1.18[c]
	$9_{1,9} \leftarrow 8_{1,8}$ F_2				

[a] The relative line strengths of these transitions were obtained from the PGOPHER simulated spectra and the absolute line intensities of these transitions could be derived relative to the measured line intensity of the HO_2 ν_2 $7_{1,6} \leftarrow 6_{1,5}$ $F_{1,2}$ transitions at 1407.620 cm^{-1}. [b] The absolute line intensities of these transitions were obtained based on the analysis of measured HO_2 and HCl spectra, and by referencing to the accurate line strength of the HCl R(9) line at 3059.316 cm^{-1}. [c] The total line strength obtained by summing the contributions from two assigned transitions.

transition at 3415.294 cm^{-1}, the ν_1 $11_{0,11} \leftarrow 11_{1,10}$ F_1 transition at 3415.363 cm^{-1}, the ν_1 $10_{0,10} \leftarrow 10_{1,9}$ F_2 transition at 3415.405 cm^{-1}, and the ν_1 $9_{0,9} \leftarrow 9_{1,8}$ F_2 and $10_{0,10} \leftarrow 10_{1,9}$ F_1 transitions at 3415.662 cm^{-1}, were observed, as shown in Fig. 5(a). In Fig. 5(b), three absorption peaks, belonging to the HO_2 ν_3 transitions, were clearly identified within the spectral range of 1122.75–1123.07 cm^{-1}. The absolute line strength of the HO_2 ν_3 $13_{1,13} \leftarrow 12_{1,12}$ $F_{1,2}$ transitions at 1122.983 cm^{-1} was previously measured to be $(1.80 \pm 0.07) \times 10^{-20}$ cm $molecule^{-1}$,[21] and was used as a reference to determine the line strengths of the HO_2 ν_1 transitions. In addition, the line strengths of the HO_2 ν_1 transitions near 3415.5 cm^{-1} were also determined by simultaneously recording the time-resolved dual-comb spectra in the range of 1407.56–1408.02 cm^{-1} and using the line strength of the HO_2 ν_2 $7_{1,6} \leftarrow 6_{1,5}$ $F_{1,2}$ transitions at 1407.620 cm^{-1} as the reference. The line strengths of HO_2 ν_1 transitions were also investigated in another range of 3456.17–3456.60 cm^{-1}. Finally, the absolute line strengths of the HO_2 ν_1 transitions were determined using the following formula:

$$S_{\nu_1} = S_{\nu_m} \times \frac{[\text{Int. } \Delta\text{Abs.}]_{\nu_1}}{[\text{Int. } \Delta\text{Abs.}]_{\nu_m}} \quad (2)$$

where S_{ν_1} represents the line strength of the HO_2 ν_1 absorption line, and S_{ν_m} represents the line strength of either the HO_2 ν_3 $13_{1,13} \leftarrow 12_{1,12}$ $F_{1,2}$ transitions at 1122.983 cm^{-1} or the HO_2 ν_2 $7_{1,6} \leftarrow 6_{1,5}$ $F_{1,2}$ transitions at 1407.620 cm^{-1}. $[\text{Int. } \Delta\text{Abs.}]_{\nu_1}$ and $[\text{Int. } \Delta\text{Abs.}]_{\nu_m}$ represent the integrated difference absorbance areas of the HO_2 ν_1 line and the ν_3 (or ν_2) line, respectively, obtained at 100–200 μs after laser photolysis. Fig. S4 (ESI†) displays the statistical distributions of multiple measurements of the line strength for the ν_1 HO_2 absorption lines in the spectral ranges of 3415.22–3415.76 cm^{-1} and 3456.17–3456.60 cm^{-1}. Table S4 (ESI†) provides a summary of the corresponding experimental conditions. Taking into account the errors from statistical and spectral analyses (2.6–6.3%), the uncertainties in the measured line strengths of the HO_2 ν_3 or ν_2 transitions (4%), and temperature uncertainty (0.2%), the absolute line strengths of the HO_2 ν_1 transitions were determined with overall uncertainties of 4.8–7.5%, depending on the SNR of each observed HO_2 peak, as listed in Table 2. Our determined ν_1 line strengths are more than three times greater than those reported in the earlier study by Zahniser *et al.*[17] and the values listed in the HITRAN database.[27]

In the vibration–rotation spectroscopic studies of HO_2 in the ν_1 vibrational band, Yamada *et al.* conducted high-resolution spectral measurements in the range of 3373–3502 cm^{-1} using a difference frequency laser source combined with the Zeeman modulation technique.[13] Approximately 280 absorption lines were assigned to be b-type transitions in the HO_2 ν_1 band, and no a-type transitions were observed. However, theoretical calculations predicted an intensity ratio of approximately 0.2 : 0.8 for a-type and b-type transitions, indicating that the contribution from a-type transitions cannot be neglected in the determination of the HO_2 ν_1 band strength. Therefore, to better evaluate the ν_1 band strength, we performed the high-resolution spectral measurements of HO_2 over a wide and continuous range from 3433.90 to 3468.90 cm^{-1}. In this experiment, to record the HO_2 spectra including the weaker a-type transitions, we employed higher initial concentrations of Cl atoms ($[Cl]_0 = 3.93 \times 10^{14}$ molecule cm^{-3}) to increase the maximum HO_2 concentration to approximately 3.4×10^{14} molecule cm^{-3}. Fig. S5 (ESI†) shows the spectra of the HO_2 recorded in the region of 3433.90–3468.90 cm^{-1}. The broadband time-dependent high-resolution spectra with an average spectral resolution of 0.002 cm^{-1} were obtained by interleaving over 200 dual-comb spectra recorded with different central wavelengths and spectral sampling spacings. In addition to the HO_2 absorption lines, numerous absorption signals

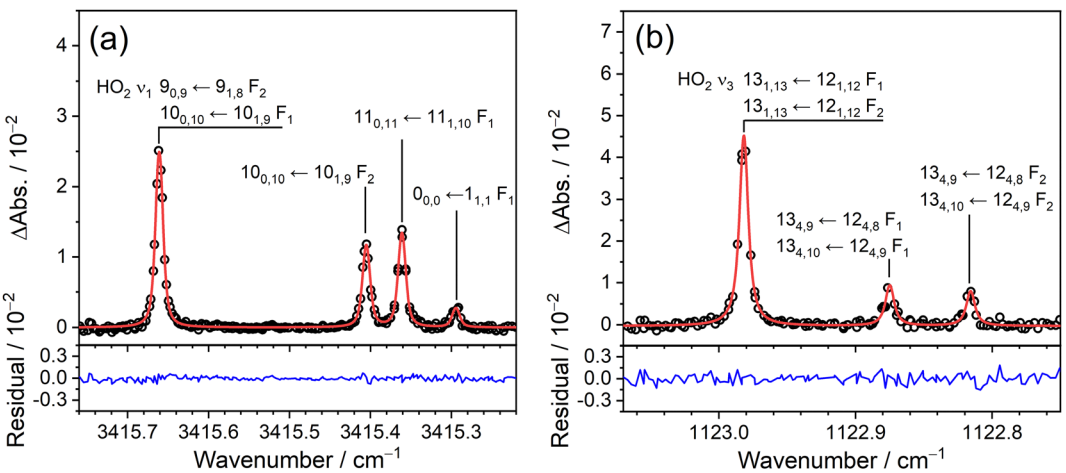

Fig. 5 High-resolution difference absorbance spectra in the regions of (a) 3415.22–3415.76 cm^{-1} and (b) 1122.75–1123.07 cm^{-1}. The spectra (black open circles) were obtained by interleaving of 4 dual-comb spectra recorded with spectral sampling spacings of 279 MHz (9.3×10^{-3} cm^{-1}) and 291 MHz (9.7×10^{-3} cm^{-1}) at 100–200 μs after photolysis of the flowing mixture of $Cl_2/CH_3OH/O_2$ (0.04/0.04/37.8 torr, P_T = 37.9 torr, and 296 K) at 351 nm with a photolysis energy of 37.7 mJ cm^{-2}. Here, the initial concentration of the Cl radical, $[Cl]_0$, is 3.03×10^{13} molecule cm^{-3}. The observed spectra were fitted using a multi-peak Voigt function (red curves) to obtain the integrated absorbance areas of the absorption peaks of HO_2 in the ν_1 and ν_3 band. The bottom panels show the fitting residuals.

Table 2 Comparison of line intensities for the HO_2 ν_1 transitions

Line position/cm^{-1}	Transition	Line intensity/10^{-21} cm molecule^{-1}			
		HITRAN[27]	Zahniser *et al.*[17]	This work *via* PGOPHER simulations[a]	This work from direct measurements[b]
3415.294	$0_{0,0} \leftarrow 1_{1,1}$ F_1	0.41		1.39	1.30 ± 0.09
3415.363	$11_{0,11} \leftarrow 11_{1,10}$ F_1	1.75		5.95	6.36 ± 0.42
3415.405	$10_{0,10} \leftarrow 10_{1,9}$ F_2	1.65		5.61	5.62 ± 0.42
3415.662	$9_{0,9} \leftarrow 9_{1,8}$ F_2 $10_{0,10} \leftarrow 10_{1,9}$ F_1	3.45[c]		11.8[c]	11.8 ± 0.63[c]
3456.302	$9_{1,8} \leftarrow 9_{0,9}$ F_1	2.08	2.3	6.99	7.34 ± 0.35
3456.360	$1_{1,1} \leftarrow 0_{0,0}$ F_1	0.46		1.55	1.41 ± 0.10
3456.563	$9_{1,8} \leftarrow 9_{0,9}$ F_2	1.87	2.1	6.28	6.24 ± 0.39

[a] The relative line strengths of these transitions were obtained from the PGOPHER simulated spectra and the absolute line intensities of these transitions could be derived relative to the measured line intensity of the HO_2 ν_1 $9_{0,9} \leftarrow 9_{1,8}$ F_2 and $10_{0,10} \leftarrow 10_{1,9}$ F_1 transitions at 3415.662 cm^{-1}. [b] The absolute line intensities of these transitions were obtained based on the spectral analysis of measured HO_2 ν_1 and ν_3 or ν_2 absorption lines, and by referencing to the well-determined line strengths of the HO_2 ν_3 $13_{1,13} \leftarrow 12_{1,12}$ $F_{1,2}$ transitions at 1122.983 cm^{-1} or the HO_2 ν_2 $7_{1,6} \leftarrow 6_{1,5}$ $F_{1,2}$ transitions at 1407.620 cm^{-1}. [c] The total line strength obtained by summing the contributions from two assigned transitions.

from the byproduct such as HCHO and the HO_2 self-reaction product, H_2O_2, were also observed in this spectral range. To obtain a clear spectral pattern of HO_2, we processed the data by subtraction of the spectra of 5.9–6.0 ms from the spectra of 0.1–0.2 ms, as shown in Fig. S5(c) (ESI†). In the processed spectra, the HCHO absorption signals were fully eliminated, and the intensity of HO_2 signals was maintained at approximately 70% of that in the early stage. However, the interferences from H_2O_2 absorption lines could not be removed and appeared as negative peaks.

Employing the PGOPHER program and using the previously reported molecular parameters of HO_2 in the ground and the ν_1 states, over 130 lines could be readily assigned to be b-type transitions in the HO_2 ν_1 band. The spectral patterns of the K_a = 1 ← 0 and 0 ← 1 sub-bands of the b-type transitions were clearly observed. For instance, in the K_a = 1 ← 0 sub-band, Q-branch transitions with $1 \leq N'' \leq 25$, R-branch lines with $0 \leq N'' \leq 8$, and P-branch lines with $2 \leq N'' \leq 17$ were clearly observed and confidently assigned. In the K_a = 0 ← 1 sub-band, we also assigned Q-branch and R-branch transitions with $1 \leq N'' \leq 15$ and $7 \leq N'' \leq 19$, respectively, in our measured range of 3433.90–3468.90 cm^{-1}. Most importantly, the spectral patterns of a-type transitions were clearly observed for the first time, and over 160 lines were assigned as a-type transitions in the HO_2 ν_1 band, with $0 \leq N'' \leq 19$ and $0 \leq K_a'' \leq 4$. By taking into account over 290 lines assigned in this work, including both a-type and b-type transitions, the vibration–rotation parameters of HO_2 in the ν_1 state were accurately determined, as summarized in Table S2 (ESI†). Fig. 6(a) shows a comparison between the observed and PGOPHER simulated spectra of HO_2 in the region of 3433.90–3468.90 cm^{-1}. Fig. 6(b) and (c) display the zoomed-in spectra in the ranges of 3459.12–3459.92 cm^{-1} and 3450.40–3451.20 cm^{-1}, respectively. By comparing the relative intensities of the a-type and b-type transitions in the processed and simulated spectra, the intensity ratio of the a- and b-type transitions was determined to be 0.18 : 0.82, which agrees well with the value predicted by theoretical calculations.

Table S5 (ESI†) summarizes the HO_2 ν_1 transitions with line strengths greater than 3×10^{-22} cm molecule^{-1} in the spectral region of 3433.90–3468.90 cm^{-1}. Fig. 7 presents a comparison of the line strengths of HO_2 ν_1 b-type transitions determined in this work with the corresponding values from the HITRAN database. The line strengths obtained in this work are higher than those in HITRAN by factors ranging from 3.37 to 3.33 across the 3433.90–3468.90 cm^{-1} region, exhibiting a linearly decreasing difference factor with increasing transition frequency, similar to the trends observed for the HO_2 ν_2 and ν_3 transitions. To further estimate the ν_1 band strength, we simulated the entire ν_1 band spectrum with the molecular parameters listed in Table S2 (ESI†) and taking into account the determined intensity ratio of the a- and b-type transitions, as shown in Fig. S6(c) (ESI†). The absolute line strengths of all individual ν_1 transitions in the range of 3060–3760 cm^{-1} could be derived by referencing the measured line strengths of the ν_1 $9_{0,9} \leftarrow 9_{1,8}$ F_2 and $10_{0,10} \leftarrow 10_{1,9}$ F_1 transitions at 3415.662 cm^{-1}. Finally, the ν_1 band strength was determined to be 18.5 ± 1.5 km mol^{-1} by summing the absolute line strengths of all ν_1 transitions over the 3060–3760 cm^{-1} range. The uncertainty (7.9%) for the ν_1 band strength was estimated by considering the standard deviation (5.7%) of the difference between the experimental values obtained from PGOPHER simulations and direct measurements, as well as the uncertainty in the determined line strength of the ν_1 $9_{0,9} \leftarrow 9_{1,8}$ F_2 and $10_{0,10} \leftarrow 10_{1,9}$ F_1 transitions (5.4%).

3.3 Comparison of experiments and quantum chemical calculations for the HO_2 band strengths

As the simplest peroxy radical, HO_2 also serves as an important reference for the characterization of organic peroxy radicals (RO_2), and its spectroscopic properties are therefore of considerable interest in both experimental and theoretical investigations. Herein, the strengths of the ν_1, ν_2 and ν_3 bands were determined to be 18.5 ± 1.5, 26.6 ± 1.3, and 22.3 ± 1.1 km mol^{-1}, respectively, based on our present and prior measurements.[21] Additionally, the dipole moment parameters for each vibrational band can also be derived using the following formula:[20]

$$S_{\mathrm{band},n} = \frac{2\pi^2 \nu_n}{3\varepsilon_0 hcQ_{\mathrm{vib}}} |\mu_n|^2 \quad (3)$$

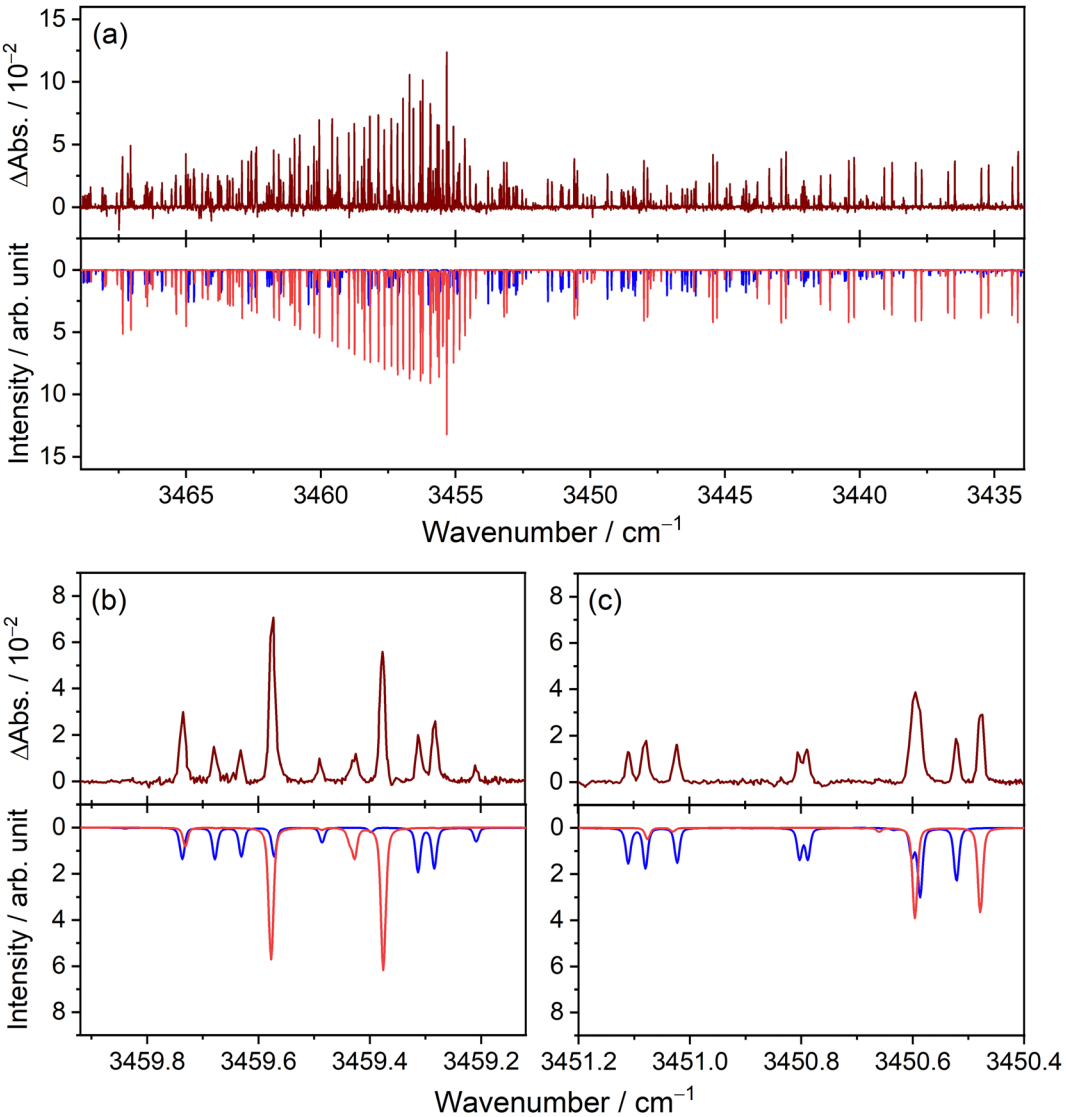

Fig. 6 Comparison of the observed and simulated spectra of HO_2 in the regions of (a) 3433.90–3468.90 cm^{-1}, (b) 3459.12–3459.92 cm^{-1}, and (c) 3450.40–3451.20 cm^{-1}. The top panels show the processed spectra obtained by subtraction of the recorded spectra of 5.9–6.0 ms from that of 0.1–0.2 ms. The bottom panels show the simulated spectra generated by the PGOPHER program with the molecular parameters listed in Table S2 (ESI†). The blue and red curves represent the a- and b-type transitions, respectively. Here, the Gaussian and Lorentzian line widths were set to be 0.007 cm^{-1} and 0.005 cm^{-1}, respectively, at 296 K. The intensity ratio for the a- and b-type transitions of the HO_2 ν_1 band is 0.18 : 0.82.

where ε_0 is the vacuum permittivity, h is the Planck constant, c is the velocity of light, ν_n represents the central frequency of each vibrational band (n = 1, 2, 3), Q_{vib} represents the vibrational partition function, and $|\mu_n|$ represents the transition dipole moment for each vibrational band. Given the central frequency of 3436.19545 cm^{-1}, 1391.75442 cm^{-1} and 1097.6250 cm^{-1} for ν_1, ν_2 and ν_3 bands, respectively, as listed in Table S2 (ESI†), the corresponding vibrational transition dipole moments $|\mu_1|$, $|\mu_2|$ and $|\mu_3|$ were determined to be (0.046 ± 0.002) D, (0.087 ± 0.002) D and (0.090 ± 0.002) D. These high-precision experimental data would be instrumental in resolving discrepancies between previous experimental and theoretical studies of HO_2 band strengths.

Table 3 summarizes the comparison of experimentally determined and calculated band strengths of HO_2 from our work and the literature. Due to the clear spectral pattern of the OO-stretching vibrational band of HO_2 and minimal interference from other reaction species in the spectral range around 9 μm, the HO_2 ν_3 transitions have been widely selected for study in experimental investigations. In early experimental studies, Buchanan *et al.* measured the HO_2 ν_3 transitions in flash lamp photolysis of $Cl_2/CH_3OH/O_2$ or $Cl_2/HCHO/O_2$ mixtures using laser absorption spectroscopy near 1117.5 cm^{-1}, and quantified HO_2 based on the formation or depletion of HCHO.[28] Later, Zahniser and Stanton determined the line strength of the HO_2 ν_3 transition near 1080 cm^{-1} and calibrated it using the measured number density of F atoms in the $F + H_2O_2 \rightarrow HO_2 + HF$ reaction system.[16] Although the results of these early experiments are mutually consistent, they are significantly lower than the values predicted by theoretical calculations.[18–20] More recently, the ν_3 band strength was revisited by Sakamoto and Tonokura as well

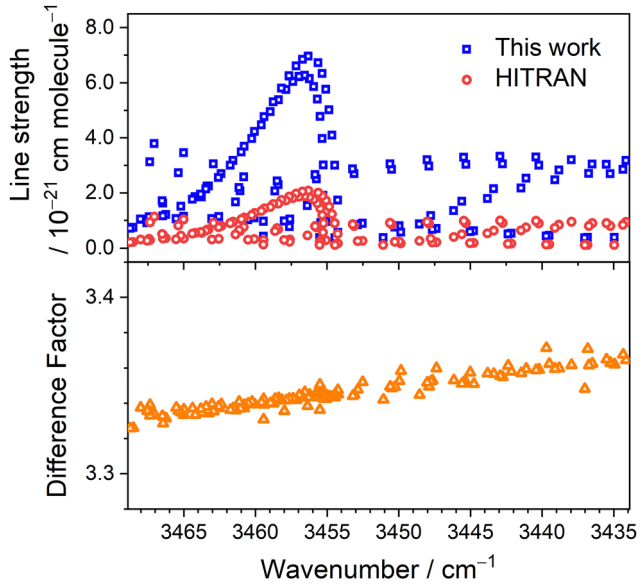

Fig. 7 Comparison of the line strengths of the HO_2 ν_1 b-type transitions determined in this work and those listed in the HITRAN database.[27] The transitions with the determined line strengths of $>3 \times 10^{-22}$ cm molecule^{-1} in the spectral region of 3433.90–3468.90 cm^{-1} are only shown here.

as in our previous work using time-resolved absorption spectroscopy with advanced laser techniques. Sakamoto and Tonokura employed quantum cascade laser absorption spectroscopy in the region near 1065 cm^{-1} to probe HO_2 ν_3 lines, quantifying HO_2 based on its reaction kinetics and the depletion of CH_3OH in the photolysis system of $Cl_2/CH_3OH/O_2$.[20] In our study, we performed simultaneous measurements of HCl and HO_2 generated by laser photolysis of $Cl_2/CH_3OH/O_2$, using synchronized two-color time-resolved dual-comb spectroscopy, and determined the HO_2 line strength relative to that of HCl.[21] Both recent experiments reported band strengths approximately three times larger than those from earlier measurements and in better agreement with quantum chemical calculations. All experimental studies were carefully conducted; nevertheless, due to instrumental limitations in early experiments, laser spectroscopy suffered from poor detection sensitivity, particularly for unstable species. To enhance the spectral signal-to-noise ratio (SNR), intensity- or frequency-modulated spectroscopy was commonly employed. However, these modulation techniques may have introduced additional and unknown systematic errors into the quantitative spectral analysis. In contrast, recent experiments have benefited from high-power laser sources and low-noise detectors, allowing time-resolved spectra to be obtained with a sufficient SNR using direct absorption methods. In particular, our two-color time-resolved dual-comb spectroscopy enables simultaneous detection of multiple species with high spectral and temporal resolutions, thereby reducing systematic errors and yielding more accurate determination of line strengths.

Compared to the ν_3 band, there have been much fewer experimental studies on the band strengths of the HO_2 ν_1 and ν_2 bands. Zahniser *et al.* determined the ν_1 and ν_2 band strengths to be 4.5 ± 1.3 km mol^{-1} and 13.0 ± 3.6 km mol^{-1}, respectively, by referencing their earlier measurement of the absolute strength of the ν_3 band.[17] These values were also smaller than those predicted by theoretical calculations. In particular, the discrepancy in the ν_1 band strengths reported by early experimental and theoretical studies is substantial, differing by a factor of 3 to 8. In this work, the ν_2 band strength was determined to be 26.6 ± 1.3 km mol^{-1}, approximately twice the value reported by Zahniser *et al.*, and more consistent with theoretical predictions, although a 30–50% discrepancy still remains. Additionally, the ν_1 band strength obtained in this work is approximately four time higher than the value reported by Zahniser *et al.*,[17] 50% higher than the calculated value reported by Dobbs and Dixon,[19] but about half the value reported by Watts *et al.*[18]

Among the early theoretical studies, Watts *et al.* benchmarked the harmonic vibrational frequencies and IR intensities for the HO_2 radical with several post-Hartree–Fock methods; their work revealed large relative differences in calculated intensities across methods.[18] Subsequently, Dobbs and Dixon demonstrated that density functional theory (DFT) methods using generalized gradient approximation (GGA) functionals may be able to predict IR intensities within a factor of two compared to experimental results.[19] However, most computational studies employ the double harmonic approximation, which introduces

Table 3 Comparison of the experimental and calculated results for the band strengths of HO_2

Methods[a]	Band strengths/km mol^{-1} ν_1	ν_2	ν_3	Ref.
laser flash photolysis coupled with TR-DCS	18.5 ± 1.5[b]	26.6 ± 1.3[c]	22.3 ± 1.1[c]	This work and Chang *et al.*[21]
Laser flash photolysis coupled with QCLAS			21.4 ± 4.2	Sakamoto and Tonokura[20]
Microwave discharge coupled with DLAS	4.5 ± 1.3	13.0 ± 3.6	7.8 ± 2.0	Zahniser *et al.*[16,17]
Flash lamp photolysis coupled with DLAS			6.7 ± 2.0	Buchanan *et al.*[28]
CCSD(T)/aug-cc-pVTZ, DVR	20.1	39.6	28.6	This work
CCSD/aug-cc-pVTZ, harmonic	35.5	42.0	31.6	This work
CCSD(T)/TZ2PF, harmonic	36.9	39.8	31.7	Watts *et al.*[18]
BP86/TZVPD, harmonic	11.8	33.8	16.8	Dobbs and Dixon[19]
B3LYP/aug-cc-pVQZ, harmonic	24.7	39.8	26.5	Sakamoto and Tonokura[20]

[a] TR-DCS: time-resolved dual-comb spectroscopy; QCLAS: quantum cascade laser absorption spectroscopy; DLAS: diode laser absorption spectroscopy; DVR: discrete variable representation. [b] Taking into account both a- and b-type transitions with the determined intensity ratio of a- and b-type transitions of 0.18 : 0.82. [c] Based on the measured high-resolution spectra, the band strength was determined considering only the a-type transitions.

notable discrepancies: the neglect of higher-order terms in the potential energy surface (PES) affects the vibrational frequencies (mechanical anharmonicity), and the assumption of a linear dipole moment introduces errors in predicted intensities (electrical anharmonicity).

To properly account for these anharmonic effects, we applied anharmonic vibrational analysis based on discrete variable representation (DVR)[29,30] methods for the HO_2 radical. The molecular geometry was optimized at the CCSD/aug-cc-pVTZ level with tight convergence criteria using the Gaussian 16 program.[31] All subsequent calculations were based on this optimized structure. To construct the potential energy surface (PES) and dipole moment surface (DMS), we used Gauss–Hermite quadrature with 7 points per mode along each of the three normal mode coordinates; for each point, we computed single-point energies at the CCSD(T)/aug-cc-pVTZ level, and dipole moments were obtained using the unrelaxed generalized density.[32] All single point calculations were performed using ORCA 6.0.0.[33]

The vibrational Hamiltonian was constructed using the Gauss–Hermite discrete variable representation (DVR), following the formulation detailed in Shizgal's monograph,[30] particularly the section on Gauss–Hermite quadrature and Sturm–Liouville eigenvalue problems. The kinetic energy matrix was evaluated using second derivatives derived from the Gauss–Hermite pseudospectral differentiation scheme and combined with the diagonal representation of the PES to form the total Hamiltonian. The resulting Hamiltonian was then diagonalized iteratively using the Lanczos method to obtain vibrational eigenstates and energies. Transition dipole integrals were computed over the DVR basis using the DMS to yield IR intensities.

According to previous literature, calculated IR intensities are generally found to be higher than experimental values. For instance, Watts *et al.* showed that post-Hartree–Fock methods with triple-ζ or larger basis sets yield IR intensities that are 1.4 to 2.0 times greater than our experimental values. Our harmonic calculations at the CCSD/aug-cc-pVTZ level, employing the linear dipole approximation, also yield IR intensities for the three bands that are comparable to those reported by Watts *et al.* Notably, the harmonic calculations incorrectly predict ν_1 to have a larger intensity than ν_3, which is inconsistent with experimental observations. In contrast, our anharmonic vibrational analysis at the CCSD(T)/aug-cc-pVTZ level reproduces the experimental trend in IR intensities among the ν_1, ν_2, and ν_3 bands, although the absolute values remain 1.1–1.5 times higher than our experimental results. Table S6 (ESI†) provides a detailed comparison of calculated vibrational frequencies and intensities. The anharmonic frequencies at the level of CCSD(T)/aug-cc-pVTZ differ from experimental values by only 4–7 cm^{-1}, indicating the high accuracy of the anharmonic treatment. In comparison, the harmonic calculations at the CCSD/aug-cc-pVTZ level show errors ranging from 25 to 50 cm^{-1}. Most importantly, we found that the choice of the generalized density is crucial for obtaining reliable DMS data: using the unrelaxed generalized density yields intensity ratios among ν_1, ν_2, and ν_3 bands that better match experimental trends; in contrast, using SCF density leads to spurious IR intensities.

On the other hand, it is noteworthy that the DFT results reported by Dobbs and Dixon predicted significantly lower IR intensities.[19] Although they claimed that their DFT results were roughly twice as high as the experimental values reported by Zahniser *et al.*, and their calculated ν_1 and ν_3 band intensities are actually lower than those obtained in our experiments. In comparison, Sakamoto and Tonokura, using B3LYP/aug-cc-pVQZ calculations,[20] reported IR intensities that are higher than those of Dobbs and Dixon and more consistent with the trends observed in our study.

Finally, to further investigate the impact of the linear dipole approximation, we extracted the third- and fourth-order derivatives of the PES, and second- and third-order derivatives of the DMS, and performed QP-VCI (quartic potential-vibrational configuration interaction) calculations.[34] When only first-order dipole derivatives were used (*i.e.*, linear dipole approximation), the band intensity ordering was $\nu_1 > \nu_3$, consistent with harmonic results. However, inclusion of second- and third-order dipole derivatives reduced the intensity of ν_1 due to opposing contributions from higher-order transition dipoles, ultimately yielding an intensity ordering consistent with experimental observations. This clearly highlights the critical role of electrical anharmonicity in producing more reliable computational IR intensities for comparison with experimental results.

4. Conclusions

In conclusion, we have conducted precise measurements of the absolute line strengths for the ν_1 and ν_2 fundamental transitions of HO_2 using synchronized two-color time-resolved dual-comb spectroscopy in the mid-infrared region. By the simultaneous detection and spectral analysis of HO_2 near 7.1 μm and the reference species HCl near 3.3 μm in the laser photolysis system of $Cl_2/CH_3OH/O_2$, the absolute line strengths of the HO_2 ν_2 transitions were determined relative to the well-known line strength of HCl. Furthermore, the absolute intensities of HO_2 ν_1 transitions were obtained by simultaneously recording the HO_2 absorption spectra in the ν_1 band and either the ν_2 or the ν_3 band, using previously established line strengths as internal references. The absolute line strengths of several HO_2 ν_1 and ν_2 transitions were experimentally determined in this work, with uncertainties as low as 4–8%. Furthermore, the ν_1 and ν_2 band strengths were accurately derived through high-resolution spectral analysis, combined with the precise vibration–rotation parameters of HO_2. These experimental values were further compared with theoretical predictions at different levels of quantum chemical theory, providing valuable benchmarks for evaluating and refining computational methods.

Overall, this work provides precise absolute line strengths for individual fundamental transitions of HO_2 in the ν_1 and ν_2 bands, along with accurate values for the corresponding band strengths. Our results contribute to improving the accuracy of

radical concentration estimates in atmospheric monitoring and laboratory kinetic studies, while also enhancing the precision and reliability of spectroscopic databases for the HO_2 radical.

Author contributions

I.-Y. Chen and C.-W. Chang performed the experiments and analyzed the data. Q.-R. Huang and J.-L. Kuo carried out the quantum chemical calculations. Q.-R. Huang wrote the section on computational methods. P.-L. Luo supervised the project, contributed to data analysis, and wrote the manuscript.

Conflicts of interest

The authors have no conflicts to disclose.

Data availability

The data supporting this article have been included as part of the ESI.†

Acknowledgements

This project is supported by the National Science and Technology Council, Taiwan (grant no. 113-2628-M-001-006-MY3 and 113-2639-M-A49-002-ASP).

References

1 D. Stone, L. K. Whalley and D. E. Heard, *Chem. Soc. Rev.*, 2012, **41**, 6348, DOI: 10.1039/c2cs35140d.
2 B. Bottorff, M. M. Lew, Y. Woo, P. Rickly, M. D. Rollings, B. Deming, D. C. Anderson, E. Wood, H. D. Alwe, D. B. Millet, A. Weinheimer, G. Tyndall, J. Ortega, S. Dusanter, T. Leonardis, J. Flynn, M. Erickson, S. Alvarez, J. C. Rivera-Rios, J. D. Shutter, F. Keutsch, D. Helmig, W. Wang, H. M. Allen, J. H. Slade, P. B. Shepson, S. Bertman and P. S. Stevens, *Atmos. Chem. Phys.*, 2023, **23**, 10287–10311, DOI: 10.5194/acp-23-10287-2023.
3 R. Woodward-Massey, R. Sommariva, L. K. Whalley, D. R. Cryer, T. Ingham, W. J. Bloss, S. M. Ball, S. Cox, J. D. Lee, C. P. Reed, L. R. Crilley, L. J. Kramer, B. J. Bandy, G. L. Forster, C. E. Reeves, P. S. Monks and D. E. Heard, *Atmos. Chem. Phys.*, 2023, **23**, 14393–14424, DOI: 10.5194/acp-23-14393-2023.
4 L. K. Whalley, K. L. Furneaux, A. Goddard, J. D. Lee, A. Mahajan, H. Oetjen, K. A. Read, N. Kaaden, L. J. Carpenter, A. C. Lewis, J. M. C. Plane, E. S. Saltzman, A. Wiedensohler and D. E. Heard, *Atmos. Chem. Phys.*, 2010, **10**, 1555–1576, DOI: 10.5194/acp-10-1555-2010.
5 X. Ren, H. Harder, M. Martinez, R. L. Lesher, A. Oliger, J. B. Simpas, W. H. Brune, J. J. Schwab, K. L. Demerjian, Y. He, X. Zhou and H. Gao, *Atmos. Environ.*, 2003, **37**, 3639–3651, DOI: 10.1016/S1352-2310(03)00459-X.
6 E. Assaf, L. Sheps, L. Whalley, D. Heard, A. Tomas, C. Schoemaecker and C. Fittschen, *Environ. Sci. Technol.*, 2017, **51**, 2170–2177, DOI: 10.1021/acs.est.6b06265.
7 A. O. Hui, M. Fradet, M. Okumura and S. P. Sander, *J. Phys. Chem. A*, 2019, **123**, 3655–3671, DOI: 10.1021/acs.jpca.9b00442.
8 I.-Y. Chen, C.-W. Chang, C. Fittschen and P.-L. Luo, *J. Phys. Chem. Lett.*, 2024, **15**, 3733, DOI: 10.1021/acs.jpclett.4c00494.
9 O. J. Nielsen, M. S. Johnson, T. J. Wallington, L. K. Christensen and J. Platz, *Int. J. Chem. Kinet.*, 2002, **34**, 283–291, DOI: 10.1002/kin.10037.
10 E. Assaf, O. Votava, S. Batut, C. Schoemaeker and C. Fittschen, *J. Quant. Spectrosc. Radiat. Transfer*, 2017, **201**, 161–170, DOI: 10.1016/j.jqsrt.2017.07.004.
11 K. Nagai, Y. Endo and E. Hirota, *J. Mol. Spectrosc.*, 1981, **89**, 520–527, DOI: 10.1016/0022-2852(81)90044-8.
12 J. B. Burkholder, P. D. Hammer and C. J. Howard, *J. Mol. Spectrosc.*, 1992, **151**, 493–512, DOI: 10.1016/0022-2852(92)90582-9.
13 C. Yamada, Y. Endo and E. Hirota, *J. Chem. Phys.*, 1983, **78**, 4379–4384, DOI: 10.1063/1.445321.
14 D. D. Nelson Jr. and M. S. Zahniser, *J. Mol. Spectrosc.*, 1991, **150**, 527–534, DOI: 10.1016/0022-2852(91)90247-8.
15 A. Charo and F. C. De Lucia, *J. Mol. Spectrosc.*, 1982, **94**, 426–436, DOI: 10.1016/0022-2852(82)90018-2.
16 M. S. Zahniser and A. C. Stanton, *J. Chem. Phys.*, 1984, **80**, 4951–4960, DOI: 10.1063/1.446517.
17 M. S. Zahniser, K. E. McCurdy and A. C. Stanton, *J. Phys. Chem.*, 1989, **93**, 1065–1070, DOI: 10.1021/j100340a010.
18 J. D. Watts, J. Gauss and R. J. Bartlett, *Chem. Phys. Lett.*, 1992, **200**, 1–7, DOI: 10.1016/0009-2614(92)87036-O.
19 K. D. Dobbs and D. A. Dixon, *J. Phys. Chem.*, 1994, **98**, 4498–4504, DOI: 10.1021/j100068a004.
20 Y. Sakamoto and K. Tonokura, *J. Phys. Chem. A*, 2012, **116**, 215–222, DOI: 10.1021/jp207477n.
21 C.-W. Chang, I.-Y. Chen and P.-L. Luo, *J. Chem. Phys.*, 2025, **162**, 034302, DOI: 10.1063/5.0244391.
22 P.-L. Luo, *Opt. Lett.*, 2020, **45**, 6791–6794, DOI: 10.1364/OL.413754.
23 P.-L. Luo and I.-Y. Chen, *Anal. Chem.*, 2022, **94**, 5752–5759, DOI: 10.1021/acs.analchem.1c04583.
24 C.-W. Chang, I.-Y. Chen, C. Fittschen and P.-L. Luo, *J. Chem. Phys.*, 2023, **159**, 184203, DOI: 10.1063/5.0176311.
25 A. S. Pine, A. Fried and J. W. Elkins, *J. Mol. Spectrosc.*, 1985, **109**, 30–45, DOI: 10.1016/0022-2852(85)90049-9.
26 C. M. Western, *J. Quant. Spectrosc. Radiat. Transfer*, 2017, **186**, 221–242, DOI: 10.1016/j.jqsrt.2016.04.010.
27 I. E. Gordon, *et al.*, *J. Quant. Spectrosc. Radiat. Transfer*, 2022, **277**, 107949.
28 J. W. Buchanan, B. A. Thrush and G. S. Tyndall, *Chem. Phys. Lett.*, 1983, **103**, 167–172, DOI: 10.1016/0009-2614(83)87487-9.
29 J. C. Light and T. Carrington Jr., in *Adv. Chem. Phys.*, ed. I. Prigogine and S. A. Rice, Wiley, 2000, 114, pp. 263–310. , DOI: 10.1002/9780470141731.ch4.
30 B. Shizgal, *Spectral Methods in Chemistry and Physics: Applications to Kinetic Theory and Quantum Mechanics*, Springer, Netherlands, Dordrecht, 2015, pp. 109–186.

31 M. J. Frisch, G. W. Trucks and H. B. Schlegel, *et al.*, *Gaussian 16, Revision C.01*, Gaussian, Inc., Wallingford CT, 2016.
32 D. Datta, S. Kossmann and F. Neese, *J. Chem. Phys.*, 2016, **145**, 114101, DOI: **10.1063/1.4962369**.
33 F. Neese, *Wiley Interdiscip. Rev.: Comput. Mol. Sci.*, 2012, **2**, 73–78, DOI: **10.1002/wcms.81**.
34 K.-L. Ho, L.-Y. Lee, M. Katada, A. Fujii and J.-L. Kuo, *Phys. Chem. Chem. Phys.*, 2016, **18**, 30498–30506, DOI: **10.1039/C6CP05537K**.